Molecular Therapy
Oncolytics
Original Article

Treatment with the PPARα agonist fenofibrate improves the efficacy of CD8+ T cell therapy for melanoma

Mohadeseh Hasanpourghadi,[1] Arezki Chekaoui,[1] Sophia Kurian,[1] Raj Kurupati,[1,2] Robert Ambrose,[1] Wynetta Giles-Davis,[1] Amara Saha,[1] Xu Xiaowei,[3] and Hildegund C.J. Ertl[1]

[1]The Wistar Institute, Philadelphia, PA 19104, USA; [2]The Janssen Pharmaceutical Companies of Johnson & Johnson, New Brunswick, NJ, USA; [3]Pathology and Laboratory Medicine, Hospital of the University of Pennsylvania, Philadelphia, PA, USA

Adoptive transfer of tumor antigen-specific CD8+ T cells can limit tumor progression but is hampered by the T cells' rapid functional impairment within the tumor microenvironment (TME). This is in part caused by metabolic stress due to lack of oxygen and glucose. Here, we report that fenofibrate treatment of human *ex vivo* expanded tumor-infiltrating lymphocytes (TILs) improves their ability to limit melanoma progression in a patient-derived xenograft (PDX) mouse model. TILs treated with fenofibrate, a peroxisome proliferator receptor alpha (PPARα) agonist, switch from glycolysis to fatty acid oxidation (FAO) and increase the ability to slow the progression of autologous melanomas in mice with freshly transplanted human tumor fragments or injected with tumor cell lines established from the patients' melanomas and *ex vivo* expanded TILs.

INTRODUCTION

Melanoma is the most lethal type of skin cancer, with a mere 22.5% 5-year survival rate for stage IV metastatic disease. Irradiation therapy and chemotherapy are not very effective[1] and have largely been replaced by targeted therapies such as B-RAF and Mitogen-Activated Protein Kinase (MAPK) inhibitors[2–4] or immunotherapies including checkpoint blockers[5–8] or adoptively transferred T cells directed against antigens expressed by the melanoma cells.[9–12] T cell therapies include transfer of *ex vivo* expanded tumor-infiltrating lymphocytes (TILs), which, as polyclonal populations, recognize multiple tumor-associated antigens. Response rates to TIL transfer are below 50% and even lower if given after treatments with anti-programmed death (PD)-1 antibodies or MAPK inhibitors,[11] Alternatively, treatments with chimeric antigen receptor (CAR)-T cells with specificity against different melanoma-associated antigens are being explored.[11] Response rates to CAR-T cell transfer vary from 20% to 51% depending on concomitant treatment with interleukins (ILs) or non-myeloablative lymphodepleting agents and the CAR-T cell receptors' specificity.[13]

TILs and CAR-T cells achieve a delay in tumor progression and in some cases full remission by causing tumor cell death through release of lytic enzyme or interactions between Fas on T cells and Fas ligand on melanoma cells. Lack of efficacy of transferred T cells could reflect that melanoma cells downregulate expression of the T cells' target antigens, that some melanoma cells are relatively resistant to T cell-mediated lysis, that T cells fail to migrate and infiltrate the melanoma lesions, and that they are suppressed within the tumor microenvironment (TME) by regulatory T cells, myeloid suppressor cells, and cancer-associated fibroblasts.[13–16] In addition, once T cells penetrate the TME, they are faced with areas of hypoxia due to incomplete vessel formation[17] and hypoglycemia due to ferocious glucose consumption by rapidly growing tumor cells.[18] These metabolic challenges further drive T cell exhaustion and loss of functions.[17]

Here, we show in a patient-derived xenograft (PDX) melanoma model[19,20] that a combination of *in vitro* and *in vivo* treatments of CD8+ TILs with fenofibrate (FF), a peroxisome proliferator receptor alpha (PPARα) agonist that switches T cell metabolism from glycolysis to fatty acid oxidation (FAO), improves their survival and functions and thereby enhances their ability to slow tumor progression.

RESULTS

The effect of a PPARα agonist on melanoma growth in a PDX model

To assess the effect of FF on human melanomas and melanoma-infiltrating lymphocytes, we used a PDX model in which human melanoma fragments were transplanted into immunodeficient NOD SCID (NSG) mice. Fresh primary or recurrent melanoma or melanoma metastasis samples (n = 12, A–Q) obtained within hours after surgery were cut into small pieces, which were transplanted each under the skin of four or five NSG mice (Figure 1A). Tumor growth was observed after transplantation of nine (D, E, G, I, M–Q) of 12 melanoma samples and tumors typically became visible within 3–8 weeks (Figure 1B). Once tumors reached a size of ∼0.5–1 cm in diameter,

Received 31 July 2023; accepted 31 October 2023;
https://doi.org/10.1016/j.omto.2023.100744.

Correspondence: Hildegund C.J. Ertl, The Wistar Institute, Philadelphia, PA 19104, USA.
E-mail: ertl@wistar.org

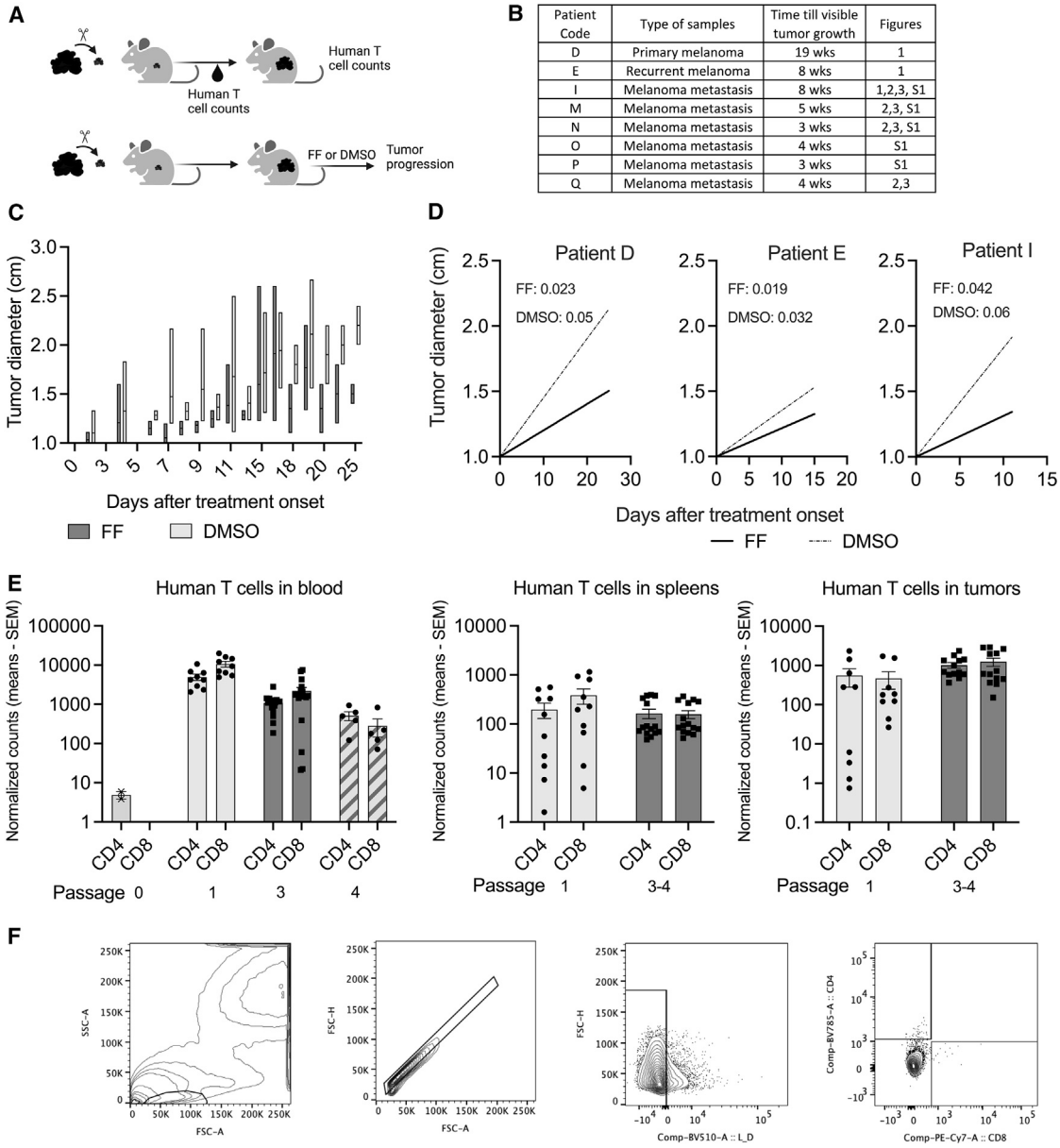

Patient Code	Type of samples	Time till visible tumor growth	Figures
D	Primary melanoma	19 wks	1
E	Recurrent melanoma	8 wks	1
I	Melanoma metastasis	8 wks	1,2,3, S1
M	Melanoma metastasis	5 wks	2,3, S1
N	Melanoma metastasis	3 wks	2,3, S1
O	Melanoma metastasis	4 wks	S1
P	Melanoma metastasis	3 wks	S1
Q	Melanoma metastasis	4 wks	2,3

Figure 1. Effect of FF on human melanoma growth in a PDX model

(A) Experimental design. (B) Patient samples (Figure S1). (C) Progression of tumor fragments from patients D, E, and I in NSG mice treated with FF or DMSO. (D) Same data as in (C) but shown as linear regression curves of tumor diameter in centimeters over time for samples from individual patients. Data were normalized to a diameter of 1 on day 0 of drug treatment. Numbers show average slope of the linear regression curves. (E) Numbers of human T cells in various tissues after one to four passages. Zero passage reflects control mice that did not receive tumor fragments. Numbers were normalized to 10^5 live lymphoid cells. Data are shown as means ± SEM. (F) Gating scheme for human TILs: lymphocyte gate, single-cell gate, live-cell gate, CD4/CD8 gate.

mice that had received fragments from patients D, E, and I were treated for 3 weeks orally with FF or its dimethylsulfoxide (DMSO)-containing diluent. Tumor growth was monitored. Oral FF treatment delayed progression of the primary melanoma of patient D, the recurrent melanoma of patient E, and the metastatic melanoma of patient I (Figures 1C and 1D). Mice that received tumors of patients D and E were tested for the presence of human T cells that had infiltrated the human tumors and were transplanted as part of the tumor fragments. Peripheral blood mononuclear cells (PBMCs) were tested at 6 (E) and 8 (D) weeks after transplantation and spleens and tumors were tested at euthanasia. As shown in Figure 1E, human $CD4^+$ and $CD8^+$ T cells could be detected at higher counts in blood than in spleens and tumors, which had more variable numbers. To assess if T cells remained present upon serial passages of tumors,

melanomas of patients I, M, and N, once they exceeded a volume of 2–2.5 cm^3 in NSG mice, were excised and fragments were transplanted into new NSG mice. This process was repeated once or twice more. Mice that received the third- or fourth-passage fragments were tested for human T cells in blood, spleens, and tumors. Although there was a trend for reduced T cell recovery from blood upon serial passages, numbers remained unchanged in spleens and tumors (Figure 1E). Blood of control mice that did not receive melanoma fragments had no detectable human $CD8^+$ T cells in blood and fewer than 10 cells/10^5 live lymphoid cells (data not shown) that stained non-specifically with an antibody to human CD4 using the gating strategy shown in Figure 1F. These data show that FF treatment delays tumor progression in a PDX melanoma model and that human TILs survive sequential passages of melanoma fragments.

The effect of a PPARα agonist in a human melanoma PDX model with autologous T cell transfer

Next, we isolated T cells from the initial tumor samples. Tumors from the same patients were maintained by sequential passages in NSG mice. T cells once they had been enriched for $CD8^+$ cells were expanded *in vitro* in medium containing IL-2. Mice that carried autologous tumor fragments were divided into four groups of five mice each. Group A received autologous $CD8^+$ T cells that had been pre-treated for 2 weeks *in vitro* with fenofibric acid (FA), an FF derivative that is suited for use in tissue culture, before transfer to recipient mice. These mice received addition oral treatment of FF after T cell transfer. Group B received DMSO pre-treated T cells and was then treated orally with DMSO. groups C and D were not injected with human T cells, they were only treated with FF or DMSO (Figure S1A). Mice that received fragments from patients I, N, and O showed reduced tumor growth if they were given T cells with FF compared to mice that only received the drug or its diluent. Mice with fragments from patient M benefited from FF regardless of $CD8^+$ T cell transfer (Figures S1B and S1C).

We isolated TILs at euthanasia from spleens and tumors from mice of groups A–C. Flow cytometric analyses revealed that overall recovery of live lymphoid cells was highest from tumors of mice that received $CD8^+$ T cells and FF and there was also a significant difference between mice of groups B and C. Mice showed low recovery of human $CD8^+$ T cells from spleens and there was no difference between mice of the three groups (A–C). Most striking were results obtained with TILs; recovery of $CD8^+$ T cells from tumors was significantly higher in group A than groups B and C and there were no significant differences between groups B and C, indicating that, without FF, the transferred T cells had either not migrated to the tumors or, more likely, that they had not survived within the TME (Figure S1D). It is also noteworthy that small numbers of $CD8^+$ TILs could be recovered from group C; these mice had not received *ex vivo* expanded T cells, indicating that the cells originated from the serially transplanted tumor samples as already shown in Figure 1. Some mice that received FF, such as those that received tumor fragments from patient N, had reduced tumor progression. TILs of groups A and B were tested by quantitative reverse transcriptase polymerase chain reaction (qRT-PCR) for transcripts encoding enzymes that play a role in different metabolic pathways. TILs from group A in comparison to group B showed modest increases in transcripts involved in fatty acid metabolism, i.e., carnitine palmitoyltransferase I (CPT-1), which is instrumental to transport fatty acids into mitochondria; PPARα, the master regulator of fatty acid metabolism; and D-beta-hydroxybutyrate dehydrogenase (BDH), an enzyme that is involved in catabolism of ketone bodies. TILs from patient I in addition showed a reduction in transcripts for some of the glycolytic enzymes (Figure S1D).

Overall, these results confirm the first set of studies showing that FF slows tumor progression. Nevertheless, the results do not allow us to conclude that reduced tumor progression is caused by metabolic changes within $CD8^+$ T cells or alternatively by a direct effect of the drug on tumor growth as, even after several passages, T cells were transferred alongside the melanoma fragments.

To measure the effects of FF on the ability of *ex vivo* expanded TILs to delay tumor progression without potential interference by TILs that had been passaged with the melanoma fragments, we established tumor cell lines from the melanomas of patients I, M, N, and Q. After expansion, 1.5×10^5 of each set of tumor cells were injected into four groups of NSG mice. $CD8^+$ TILs from the same patients were expanded *in vitro* using medium containing both IL-2 and IL-15. T cells were treated for 2 weeks with FA or DMSO and then transferred into two groups of mice (A and B) that carried visible tumors (~0.2 cm in diameter). Mice of group A were further treated with FF, and mice of group B received DMSO. Groups C and D were treated with FF or DMSO, respectively, but did not receive T cells (Figure 2A). Samples from the different patients showed comparable patterns so we combined their data for most of the statistical analyses. Tumor growth was significantly slower in group A compared to the other three groups, indicating that the delay in tumor progression was caused by the combination of FF and the transferred $CD8^+$ T cells. Small differences were also seen between groups C and D, suggesting that FF by itself has a modest effect on tumor progression, and groups B and D, indicating an effect of transferred $CD8^+$ T cells even when they were left untreated (Figures 2B–2D). Mice were euthanized once tumors exceeded a volume of ~2–2.5 cm^3 and survival time was recorded. Regardless of the tumors' origin, only group A showed an increase in survival time (Figure 2E). An analysis of splenocytes and TILs again showed higher recovery of live lymphoid cells from tumors of group A compared to the other three groups (Figure 3A). There was a trend in groups A and B toward higher recovery of $CD8^+$ T cells from tumors than spleens. Group A had significantly higher $CD8^+$ TIL counts compared to the other groups. Although some $CD8^+$ T cells could be recovered from group B, this failed to reach significance compared to the low numbers of cells that exhibited non-specific staining in groups C and D. T cells were tested for production of interferon (IFN)-γ; 80%–90% of $CD8^+$ T cells from group A produced this cytokine. IFN-γ production was less frequent in $CD8^+$ T cells from group B, suggesting that FF preserved T cell functions (Figure 3A). Immunohistology from tumors

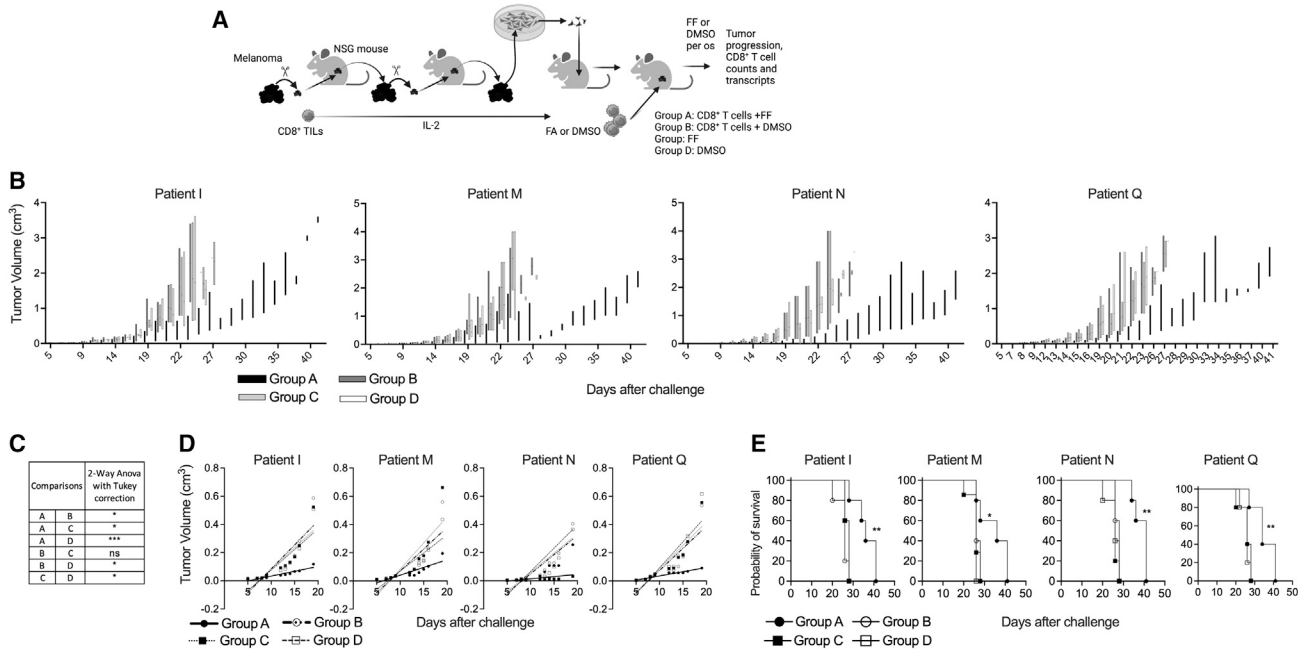

Figure 2. Effect of FF on the ability of transferred CD8$^+$ TILs to slow tumor progression

(A) Experimental design. (B) Progression of tumors from the indicated patients in the four different treatment groups. (C) Same data as in (B) shown as linear regression curves. Data next to the graphs show the results of comparing the slope of the curves of individual mice by Fisher's least significant difference (LSD) test. (D) Tumor progression shown as linear regression lines for tumor volume over time. (E) Kaplan-Meier survival graphs for the different groups receiving tumor cells from the indicated patients. Data were compared by Mantel-Cox test.

confirmed the data obtained by flow cytometry (Figure 3B); those of group A were heavily infiltrated by human CD8$^+$ T cells that accumulated at the border between healthy and necrotic tumor tissue (Figure 3C), while CD8$^+$ T cells were rare in tumors of group B. Those that could be detected in group B tumors commonly showed membrane blebbing, which is typically associated with apoptosis (Figure 3D).

CD8$^+$ T cells from mice with sufficient lymphocyte recovery were tested for exhaustion/differentiation markers (Figure 3E). Percentages of PD-1$^+$CD8$^+$ cells from TILs were higher in group A than B tumors or group A spleens. Expression of lymphocyte-activating protein (LAG-3) was not increased, while percentages of cytotoxic T lymphocyte-associated protein 4 (CTLA-4) were increased in group A tumors compared to spleens. In tumors, especially those from group A, triple-positive CD8$^+$ T cells were most common (Figure 3F).

TILs from groups A and B as well as tumor cells from groups C and D were tested for transcripts encoding metabolic enzymes. Samples from the four different patients showed comparable patterns. Group A T cells compared to group B T cells showed highly significant increases in transcripts for enzymes of fatty acid metabolism and decreases in those of glycolysis and histone methyltransferase (HMT), an enzyme of one-carbon metabolism (Figure 3G), as would be expected upon PPARα activation. No metabolic differences were observed between tumor cells from mice of groups C and D (Figure 3H).

The combined data of groups A and B were analyzed for correlations by Spearman. As shown in Figure 4, there were strong inverse correlations between tumor growth, represented by the slope of the linear regression curves in Figure 2, and lymphocyte, CD8$^+$, and IFN-γ$^+$CD8$^+$ T cell counts in tumors. For the cycle threshold (Cτ) values, there were strong positive correlations between tumor growth and transcripts for enzymes of fatty acid metabolism and inverse correlations between tumor growth and enzymes of glycolysis. As Cτ values are inversely related to levels of transcripts, high levels of enzymes of fatty acid metabolism combined with reduced glycolytic enzymes correlated with delayed tumor growth. Lymphocyte and T cell counts in tumors showed strong inverse correlation with the Cτ values for enzymes of fatty acid metabolism and direct correlations with those for glycolysis, indicating that preservation of the transferred T cells was linked to their switch from glycolysis to fatty acid metabolism. As expected, enzymes of a given metabolic pathway, such as glycolysis or FAO, showed strong positive correlations with each other and inverse correlation with those of the other pathway. Regarding exhaustion markers, percentages of human CD8$^+$ cells that were only positive for PD-1 inversely correlated with tumor growth and Cτ values for transcripts of enzymes involved in FAO but showed positive correlations for enzymes of glycolysis and CD8$^+$ T cell recovery. CD8$^+$ T cells that were only positive for LAG-3 showed the opposite pattern. These data indicated that PD-1, unlike LAG-3 expression on CD8$^+$ T cells, facilitated delay of tumor progression by enhancing FAO and blocking glycolysis.

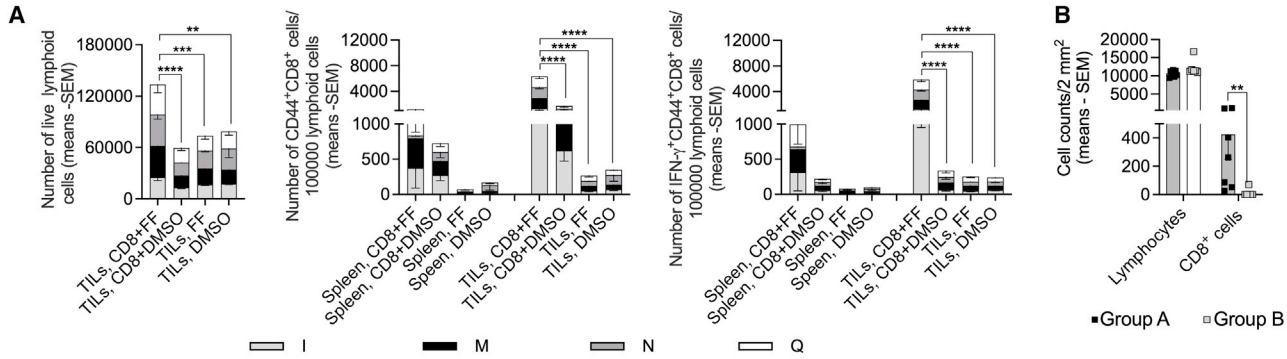

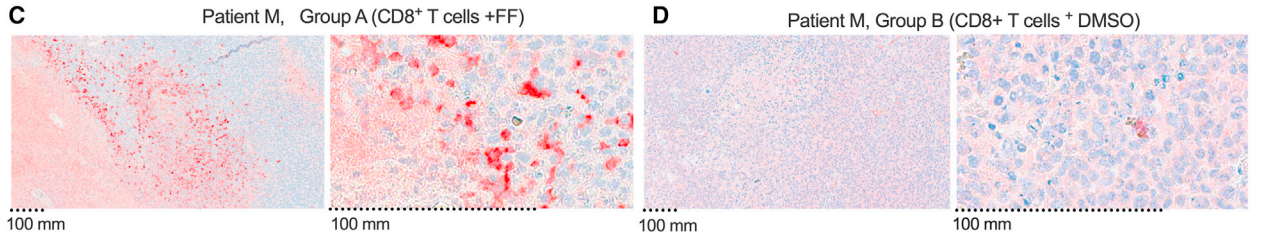

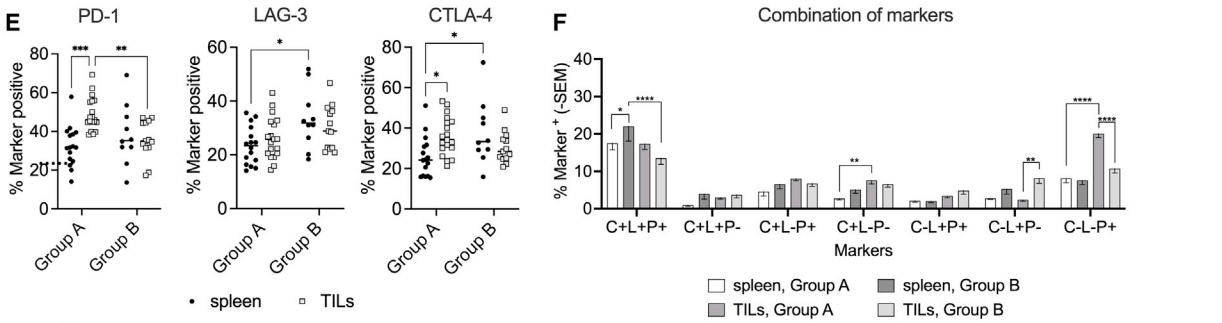

G TILs

Pathway	Enzyme	Patient I	p-values	Patient M	p-values	Patient N	p-values	Patient Q	p-values
FAO	CPT1		1.40E-07		4.10E-07		7.50E-09		8.20E-08
FAO	PRAR-alpha		1.70E-06		2.10E-05		1.70E-07		3.60E-08
FAO	BDH1		3.60E-07		2.00E-05		4.60E-06		4.60E-07
Glycolysis	HK2		0.0001		4.30E-08		8.10E-08		3.60E-08
Glycolysis	GLUT1		0.004		1.60E-05		1.60E-06		1.40E-05
Glycolysis	LDH1		0.002		5.40E-08		1.40E-08		3.50E-05
Glycolysis	GPI		0.002		0.0001		3.80E-06		6.20E-08
Glycolysis	PDHX		0.002		4.50E-06		0.0002		1.90E-07
Glycolysis	PGK1		4.30E-07		0.3		0.007		1.10E-06
1-Carbon metab.	HMT		0.006		1.60E-05		2.40E-06		1.50E-06

H Tumor cells

Pathway	Enzyme	Patient I	p-values	Patient M	p-values	Patient N	p-values	Patient Q	p-values
FAO	CPT1		0.12		0.23		0.06		0.28
FAO	PRAR-alpha		0.21		0.41		0.16		0.72
FAO	BDH1		0.30		0.85		0.62		0.26
Glycolysis	HK2		0.90		0.34		0.03		0.02
Glycolysis	GLUT1		0.92		0.78		0.05		0.68
Glycolysis	LDH1		0.23		0.83		0.05		0.43
Glycolysis	GPI		0.92		0.83		0.01		0.78
Glycolysis	PDHX		0.46		0.73		0.41		0.13
Glycolysis	PGK1		0.76		0.82		0.27		0.35
1-Carbon metab.	HMT		0.22		0.54		0.01		0.92

-10 -5 -2 0 2 5 10

Figure 3. Effect of FF on TILs transferred into cell-line-derived tumor-bearing NSG mice

(A) Recovery of lymphoid cells, human CD44$^+$CD8$^+$ T cells, and IFN-γ-producing human CD44$^+$CD8$^+$ T cells from spleens and tumors. Counts (lymphoid cells) or counts normalized to 10^5 live lymphoid cells are stacked for samples from different patients. (B) Lymphocyte and human CD8$^+$ T cell counts by immunohistochemistry. Counts are normalized to a total area of 2 mm^2. (C and D) Sections of tumors from NSG mice receiving patient M tumor cells. (C) TILs and mice treated with FA or FF. (D) TILs and mice treated with DMSO. (E) Percentages of human CD8$^+$ T cells expressing the indicated markers. (F) Percentages of cell expressing combinations of markers determined by

(legend continued on next page)

DISCUSSION

Immunotherapy by T cell transfer has achieved remarkable successes in liquid tumors; their effectiveness in solid tumors remains limited. This is at least in part caused by rapid T cell impairment within the immunosuppressive TME.[16] Resting T cells use the mitochondrial tricarboxylic acid (TCA) cycle to fuel their metabolism by glucose, amino acids, and fatty acids. Upon engagement of the T cell receptor with its cognate antigen displayed by major histocompatibility antigens and co-stimulation through ligation of CD28, $CD8^+$ T cells through activation of the phosphoinositide 3-kinase (PI3K)/protein kinase B (Akt) pathways increase expression of the glucose receptor (Glut)1 and switch their metabolism to glycolysis;[21] this in turn allows them to rapidly generate energy and building blocks for effect functions and cell divisions. As first described by Warburg, tumor cell growth is also fueled by aerobic glycolysis,[22] which depletes this nutrient from the TME. Tumor cells can outcompete T cells for glucose, and lack of this nutrient leads to reduced activity of the mammalian target of rapamycin (mTOR), which impairs cytokine production.[23] Lack of the glucose metabolite phosphoenolpyruvate, which is crucial for T cell receptor-mediation activation of nuclear factor of activated T cells (Ca^{++}NFAT), further impairs T cell functions.[24] Regulatory T cells, in contrast, are relatively unaffected by hypoglycemia as they fuel their metabolism primarily through lactate and fatty acids.[25] The tumor cells' increased secretion of lactic acid, the final metabolite of glycolysis, decreases the TME's pH, which impairs the T cells' ability to migrate, produce cytokines, or release lytic enzymes.[26] In turn, in animal models, increasing the TME's pH was shown to improve the efficacy of T cell-mediated immunotherapy.[27]

T cells in a hypoglycemic environment can switch from glycolysis to FAO,[17] which is promoted by increased expression of PD-1.[28,29] A switch to FAO in the absence of glucose does not necessarily terminate T cell activation and T cells can be stimulated and acquire effector functions, albeit less efficiently, in the absence of glucose.[30] We have previously tested FF or its derivative FA in a mouse melanoma model. FF's primary mode of action is to activate the PPARα pathway, which increases FAO and lipolysis and thereby reduces levels of triglycerides, cholesterol, and low-density lipoprotein. It also is a partial agonist of the nuclear receptor subfamily one group I member 2, which regulates metabolism and secretion of various compounds, including xenobiotics.[31] We assume that FF or its derivative FA affect tumor progression by changing the metabolism of $CD8^+$ T cells from glycolysis to FAO, which in turn preserves their effector functions within the hypoglycemic TME and provides them with a survival advantage. In contrast, others have shown that increased CD36-mediated uptake of fatty acids can blunt TIL functions.[32]

Our initial studies on the effect of FF on melanoma-penetrating T cells were conducted in immunocompetent mice that had been injected with mouse tumor cells.[17] Here, we extend the validity of these original finding to a human melanoma PDX model in which mice initially received transplants of tumor fragments from patients with metastatic or recurrent melanoma. This model has the advantage that all components of melanoma, including tumor and stromal cells as well as TIL subsets, are present and thereby mirror the human TME. In order to distinguish whether FF delayed tumor progression by negatively affecting the metabolism of tumor cells or improving TIL functions, we had to switch to the use of tumor cell lines and adoptively transferred autologous $CD8^+$ TILs. In both models, FF delayed tumor progression and, as was shown using the $CD8^+$ TIL transfer model, this was accompanied by a metabolic switch of $CD8^+$ TILs from glycolysis to FAO, as shown by declines in transcripts encoding glycolytic enzymes accompanied by increases in those involved in metabolism of fatty acid and ketone body. The latter may have been provided by tumors cells as previous studies showed that FF in a PPARα-independent way increases production and secretion of ketone bodies by melanoma cells.[33] FF-driven metabolic changes in TILs in turn correlated with increased TIL recovery from human melanoma-bearing mice and better preservation of their ability to produce IFN-γ. Although FF had previously been shown to slow progression of a transplanted mouse melanoma cell line,[34] the drug had no significant effects on growth or metabolism of human melanoma cells. Without FF treatment, only very few human $CD8^+$ TILs could be recovered from the tumors, while, in contrast, sections from mice of group A showed robust infiltration with the human TILs, which were commonly clustered around large areas of dead tumor tissue, suggesting the T cells had been able to kill the tumor cells.

Human $CD8^+$ T cells from spleens and tumors expressed exhaustion markers and ∼15%–20% were triple positive for PD-1, LAG-3, and CTLA-4. The only population that was significantly increased in group A tumors compared to spleens or group B tumors were human $CD8^+$ T cells, which only expressed PD-1. This population correlated with a delay in tumor progression and with the cells' metabolic switch from glycolysis to FAO. PD-1 signaling is known to inhibit glycolysis by reducing expression of Glut1 and the activity of hexokinase (HK)2, the first enzyme of the glycolysis pathway. Inhibition of the PI3K/Akt pathway further augments fatty acid metabolism, as supported by our correlation studies.[29] CTLA-4 has similar effects on glycolysis but fails to affect FAO,[28] and in our study it did not show strong correlations with levels of transcripts of metabolic enzymes, while increased frequencies of human $CD8^+$ T cells expressing LAG-3, which is regulated by HIF-1a and increases under hypoxia, correlated with tumor progression, decreases in enzymes of FAO, and increases in those involved in glycolysis.

Boolean gating. (A, B, E, and F) Difference were calculated by two-way ANOVA with Tukey correction; data are shown as means ± SEM. (G) Differences in Cτ values between TILs and (H) tumor cells from individual sample of groups A and averaged samples from group B are shown in a heatmap for individual mice receiving samples from the indicated patients. p values comparing the original Cτ value. (F) Differences in Cτ values between tumor cells in isolated tumor samples of group C and averaged tumor samples from group D are shown in a heatmap for individual mice receiving samples from the indicated patients. p values comparing the original Cτ values for groups C and D. (E and F) Differences were calculated by multiple unpaired t test with two stage step-up method by Benjamini, Krieger, and Yekutieli.

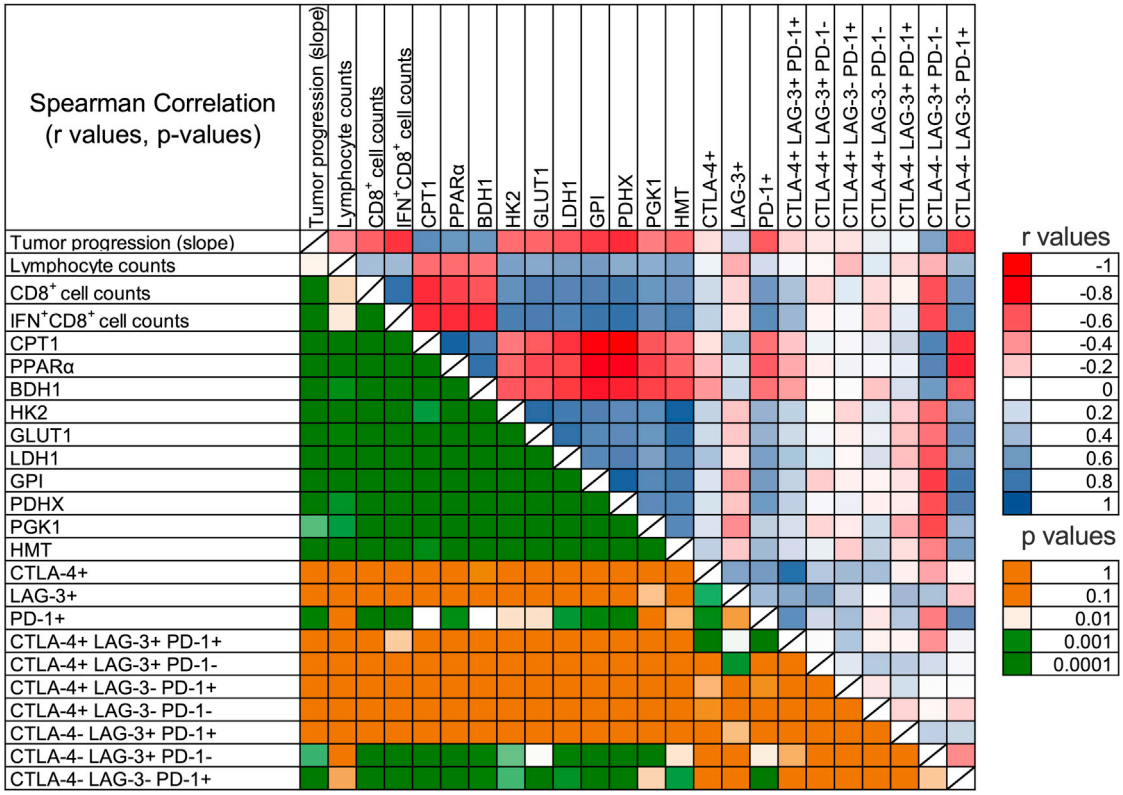

Figure 4. Correlations

Graph shows as heatmaps *r* values by Spearman correlation correlations on top with matching p values below.

Others have attempted to reduce tumor progression by addressing the TILs' metabolic defects. Endolase 1, a key glycolytic enzyme needed for production of pyruvate, was found to be defective in melanoma-infiltrating $CD8^+$ T cells, whose functions improved, at least *in vitro*, if they were cultured in medium containing pyruvate.[35] Other metabolic manipulations targeting melanoma cells, such as proton pump inhibitors, blockade of glycolysis, or FAO, may block tumor progression[36] but will most likely also impair TIL functions. Metformin is another metabolic drug that has been shown to slow tumor progression both through mTORC1-dependant and independent mechanisms and in addition to improve fitness of $CD8^+$ TILs in different types of solid cancer.[37–39]

In summary, data presented here conducted with fresh human tumor material invite further clinical studies in the use of PPARα agonist to perform the efficacy of TILs or CAR-T cells for immunotherapy of metastatic melanoma and potentially other forms of solid cancers.

MATERIALS AND METHODS

Tumor specimen from patient

Use of human melanoma samples was approved by the Wistar Institute's protocol #201441. Tumors were obtained directly after surgery from patients of Hospital of the University of Pennsylvania upon their informed consent. To protect patients' confidentiality, data of gender, age, and ethnicity were not provided to the investigators of this study.

Mice and surgical procedure

All animal procedures were approved by the Institutional Animal Care and Use Committee (IACUC) of the Wistar Institute (Philadelphia, PA, 19104). Experiments were conducted under protocols that were approved by the IACUC under protocol numbers 201335 and 201441. Male NSG mice (6–8 weeks old) were obtained from Wistar Institute Animal Facility and kept under barriers conditions suited for severely immunocompromised mice.

Transfer of fresh human tumor fragments

Tumors were cut into small pieces. NSG mice received the analgesic drug buprenorphine (1 mg/kg subcutaneously) 20–30 min before surgery. Isoflurane was administrated to anesthetize the mice. An approximately 5-mm incision was made in shaved skin of the lateral body wall posterior to the axillary area. A subcutaneous pouch was created by blunt dissection. Fresh human tumor fragments (n = 4–5) were inserted, and the incision was closed with sterile clips. Amoxicillin (Sandoz, Princeton, NJ) was given at 1.9 mL/22.7 mg in 250 mL of water orally for 14 days post surgery. Mice were under post-operative care for 2 weeks. Clips were removed 14 days post surgery and

tumors were measured using calipers five times a week. Treatment started when tumors reached ~0.5 cm^3 in volume.

Isolation of melanoma cells

Tumor fragments were suspended in Hank's balanced salt solution (HBSS) with Ca^+ and Mg^+ (Corning, NY, NY) containing 50U/mL DNase I (Sigma-Aldrich, Burlington, MA), 2 mg/mL collagenase IV (Sigma-Aldrich, Burlington, MA), and 1 mg/mL hyaluronidase V (Sigma-Aldrich, Burlington, MA) diluted in HBSS with Ca^+ and Mg^+ (Corning, NY, NY) at 37°C under agitation for 30 min. They were then filtered through 70-μm cell strainers, washed twice in HBSS, and cultured in RPMI medium containing 10% FBS. Prior to injection into mice, cells were collected, washed, and 5×10^5 cells in 100 μL of serum-free medium mixed with 100 μL of Matrigel matrix (Corning, NY, NY) were injected subcutaneously into the left flanks of mice.

Isolation of TILs

For some experiments, ~3-mm^3 tumor fragments were cultured in 24-well plates with AIMV medium (Gibco, Billings, MT) supplemented with 30 IU/mL of human IL-2 (Sigma-Aldrich, Burlington, MA), 10 ng/mL of recombinant human IL-15 (Peprotech, Cranbury, NJ), 5% human serum (Sigma-Aldrich, Burlington, MA), 100U/mL penicillin, 100 μg/mL streptomycin, 25 mmol/L HEPES, and 5.5×10^{-5} mol/L β-mercaptoethanol in a 37°C incubator with 5% CO_2. Half of the medium was replaced twice a week. After 10–14 days of culture, residual tumor fragments were removed and lymphocytes were transferred to fresh wells and cultured in medium containing 30 IU/mL of IL-2. Alternatively, tumor fragments were digested as described above and TILs were purified by Ficoll density gradient centrifugation at 2,000 rpm for 20 min at room temperature.

Enrichment of $CD8^+$ T cells

$CD8^+$ TILs were selected for by using magnetic beads of the Human $CD8^+$ T cell enrichment kit and EasySep RoboSep buffer (both Stemcell, Philadelphia, PA). $CD8^+$ were cultured in AIMV medium (Gibco, catalog #12-055-091) supplemented with 30 IU/mL of human IL-2, 10 ng/mL of recombinant human IL-15, 5% human serum 100U/mL penicillin, 100 μg/mL streptomycin, and 25 mmol/L and 5.5 × 10−5 mol/L β-mercaptoethanol. T cells of patient I grew poorly under those conditions. They were initially cultured in plates coated with 1 μg/mL of anti-human CD3 (Invitrogen, Waltham, MS; clone OKT3) and 1 μg/mL anti-human CD28 (eBioscience, San Diego, CA, clone CD28.2) in a pre-coated 96-well plate for 72 h. They were then maintained like the T cells from the other patients.

In vitro FA treatment of $CD8^+$ T cells

Human $CD8^+$ TILs were expanded as described above. Once they reached confluency, they were split into two groups and suspended in AIMV medium. One was treated with 100 μM FA in 2% DMSO (Sigma-Aldrich, Burlington, MA) and the other was treated with 2% DMSO for 14 days. AIMV medium with the additives was changed two or three times a week.

Adoptive transfer of autologous $CD8^+$ T cells

Human $CD8^+$ cells were washed and 1×10^5 cells in 100 μL of serum-free medium with 30 IU/mL IL-2 were injected subcutaneously close to the growing tumors. The control group received 100 μL of serum-free medium instead.

FF treatment of mice

FF (Sigma-Aldrich, Burlington, MA) at 100 mg/kg/day in PBS containing 2% DMSO was given orally to mice daily for 3–4 weeks and 1× PBS. Control mice received PBS with 2% DMSO. Treatment began when tumors reached 0.5 cm in diameter and was stopped when tumors reached about 1.5–2 cm. Tumor volume was measured five times a week and calculated according to the formula: $^1/_2$ (length × ($width^2$)). Tumors were excised once they exceeded a volume of 2.5–3.5 cm^3.

RNA extraction, cDNA synthesis and qPCR

Tumors were collected from euthanized mice, digested as described above, TILs were purified, and RNA was isolated using TRIzol reagent (Invitrogen, Waltham, MA). RNAs were resuspended in 20 μL of diethylpyrocarbonate-treated water and treated with DNase I (Sigma-Aldrich, Burlington, MA) and RNasin Plus (Promega, Madison, WI). Samples were incubated at 37°C for 20 min and then run on a thermal cycler (Eppendorf Mastercycler) at 75°C for 10 min. The purity of RNA samples was assessed by measuring UV absorbance at A260 (260 nm).

Complimentary DNA (cDNA) was synthetized using the high-capacity cDNA reverse transcription kit (Applied Biosystems, Wilmington, DE) according to the manufacturer's protocol. Minus-RT control without reverse transcriptase was generated along with RNA samples to ensure lack of DNA contamination. The qRT-PCR was conducted in duplicates with Powerup SYBR Green Master Mix (Applied Biosystems, Wilmington, DE) using the 7500 standard mode Real-Time PCR system (Applied Biosystems, Wilmington, DE). Selected primers of metabolic markers to amplify the cDNA were CPT1, HK2, BDH, LDH1, PRAR-alpha, GLUT1, PGK1, GPI, and PDHX using the following primers:

CPT1A: forward (F), TCCAGTTGGCTTATCGTGGTG; reverse (R), TCCAGAGTCCGATTGATTTTTGC.

HK2: F, AACAGCCTGGACGAGAGCAT; R, GCCAACAATGAG GCCAACTT.

BDH1: F, GACAGCCTAAACAGTGACCGA; R, GAGCGGACAAT CTCCACCA.

LDH1α: F, AGCTGTTCCACTTAAGGCCC; R, TGGAACCAAAAG GAATCGGGA.

PPARα: F, GGCAAGACAAGCTCAGAAC; R, TTATCTATGAAGC AGGAAGCA.

GLUT1: F, ATTGGCTCCGGTATCGTCAAC; R, GCTCAGATAG GACATCCAGGGTA.

PGK1: F, TAAAGGGAAGCGGGTCGTT; R, GTGGCTCATAAG GACTACCGACTT.

GPI: F, GATGGTAGCTCTCTGCAGCC; R, GCCATGGCGGGAC TCTTG.

PDHX: F, GAGTGGTTGATGACGAACTGG; R, GGCAAGTCGGA TAGGATTCTCTA.

HMT: F, CAATGACGATGCCAGTCAA; R, GAGGGGTTGTGCC AGCA; 1.

8SrRNA: F, GTAACCCGTTGAACCCCATT; R, CCATCCAATCG GTAGTAGCG.

Normalized Cτ values were used to compare levels of transcripts.

Isolation of lymphocytes from spleens

Lymphocytes were isolated from spleen of mice as described before.[40]

Surface marker and intracellular cytokine staining

Lymphocytes from tumors and spleens were stained with APC-labeled anti-human CD8 (eBioscience, San Diego CA, clone RPA-T8), BV605-labeled anti-human CD4 (BD Biosciences, San Jose, CA, clone SK3), Alexa Fluor 700 anti-human CD44 (BioLegend, San Diego, CA, clone BJ18), PE anti-human PD1 (BioLegend, San Diego, CA, clone EH12.2H7), Alexa Fluor 647 anti-human LAG3 (BioLegend, San Diego, CA, clone 11C3C65), and PerCP/Cyanine5.5-labeled anti-human CTLA-4 (BioLegend, San Diego, CA, clone L3D10) at 1 min 100 μL of cell staining buffer (BioLegend, San Diego, CA). Live/dead fixable violet dead cell stain (Invitrogen, Waltham, MA) was diluted at 1 in 400 μL cell staining buffer. Cells were incubated with antibodies at 4°C for 30 min. Next, cells were washed with cell staining buffer, fixed, and permeabilized with BD cytofix/cytoperm (BD Biosciences, San Jose, CA) at 4°C for 20 min. Then cells were washed with BD perm/wash (BD Biosciences, San Jose, CA) and stained with fluorescein isothiocyanate (FITC)-labeled anti-human IFN-γ (BioLegend, San Diego, CA) at 4°C for 30 min followed by washing the cells once and analyzing them by BD FACSCelesta Cell Analyzer (BD Biosciences, San Diego, CA). Data were calculated by FlowJo (TreeStar, Woodburn, OR).

Immunohistochemistry

The 4-μm sections of paraffin-embedded tumors were mounted on charged slides and baked at 60°C for 1 h. Sections were deparaffinized and rehydrated in two consecutive changes of xylene substitute, 100% ethanol (EtOH), 95% EtOH, and deionized water. Hydrophobic barriers were drawn around the tissue sections with a Vector ImmEdge pen. Antigen retrieval was achieved with DAKO EDT (pH 9) under pressure at 110°C for 10 min. Slides were cooled on the counter for 20 min and rinsed with water. They were immersed in a 3% hydrogen peroxide solution for 10 min then rinsed in water. First, primary anti-CD8 antibody (Cell Signaling Technology, Danvers, MA) diluted with Cell Signaling Technology Signal Stain Ab diluent was applied to tissue sections and incubated overnight at 4°C. After rinsing, secondary antibody (Vector horseradish peroxidase [HRP] anti-rabbit polymer) was applied to all sections and incubated for 30 min at room temperature. AEC (red) Vector peroxidase was applied for 30 min. Control sections were only treated with the second antibody and the substrate.

Sections were analyzed with Nikon Eclipse Ti Inverted Microscope, Light Engine SOLA SE II 365, PSF (Perfect Focus System), Motorized FL Filter Turret, Prior Stage, Piezo Stage, using a Nikon 20× Plan Apo, numerical aperture (NA) 0.95 objective and the Nikon NIS Elements AR Version 5.30.02 (Build 1545) software.

Statistical analysis

All statistical analyses were conducted using GraphPad Prism 6 (GraphPad, San Diego, CA). Differences between two populations were calculated by Student's t test. Multiple comparisons between two groups were performed by multiple t test with type I error correction. Differences among multiple populations were calculated by one- or two-way ANOVA. Differences in survival were calculated by log rank Mantel-Cox test. Differences between tumor growth curves were determined by repeated measures two-way ANOVA. Type I errors were corrected by the Holm-Šídák method. Significance was set at p values of or below 0.05. For all figures, *$p \leq 0.05$–0.01, **$p \leq 0.01$–0.001, ***$p \leq 0.001$–0.0001, and ****$p \leq 0.0001$. Unless noted in the figure legend, all data are shown as mean ± SEM.

DATA AND CODE AVAILABILITY

All data are available in the main text or the supplemental information.

SUPPLEMENTAL INFORMATION

Supplemental information can be found online at https://doi.org/10.1016/j.omto.2023.100744.

ACKNOWLEDGMENTS

This work was funded by a grant from the Department of Defense, United States (# W81XWH-19-1-0485 CA180191). We wish to thank Ms. Cole for assistance in finalizing the manuscript.

AUTHOR CONTRIBUTIONS

M.H., A.C., S.K., R.K., R.A., W.G.-D., A.S., X.X., and H.C.J.E. authored the manuscript. H.C.J.E. is responsible for conceptualization. M.H., R.K., and A.C. are responsible for the methodology. M.H., A.C., S.K., R.A., W.G.-D., A.S., and X.X. carried out the investigation. H.C.J.E. raised the funding and conducted the project administration. M.H. and H.C.J.E. supervised and wrote the original draft of the manuscript. R.K. contributed to editing the manuscript.

DECLARATION OF INTERESTS

The authors declare no competing interests.

REFERENCES

1. Pham, J.P., Joshua, A.M., Da Silva, I.P., Dummer, R., and Goldinger, S.M. (2023). Chemotherapy in cutaneous melanoma: Is there still a role? Curr. Oncol. Rep. *25*, 609–621.
2. Larkin, J., Ascierto, P.A., Dréno, B., Atkinson, V., Liszkay, G., Maio, M., Mandalà, M., Demidov, L., Stroyakovskiy, D., Thomas, L., et al. (2014). Combined Vemurafenib and Cobimetinib in BRAF- mutated melanoma. N. Engl. J. Med. *371*, 1867–1876.
3. Long, G.V., Flaherty, K.T., Stroyakovskiy, D., Gogas, H., Levchenko, E., De Braud, F., Larkin, J., Garbe, C., Jouary, T., Hauschild, A., et al. (2017). Dabrafenib plus trametinib versus dabrafenib monotherapy in patients with metastatic BRAF V600E/K-mutant melanoma: long-term survival and safety analysis of a phase 3 study. Ann. Oncol. *28*, 1631–1639.
4. Wahid, M., Jawed, A., Mandal, R.K., Dar, S.A., Akhter, N., Somvanshi, P., Khan, F., Lohani, M., Areeshi, M.Y., and Haque, S. (2018). Recent developments and obstacles in the treatment of melanoma with BRAF and MEK inhibitors. Crit. Rev. Oncol. Hematol. *125*, 84–88.
5. Robert, C., Thomas, L., Bondarenko, I., O'Day, S., Weber, J., Garbe, C., Lebbe, C., Baurain, J.-F., Testori, A., Grob, J.-J., et al. (2011). Ipilimumab plus Dacarbazine for previously untreated metastatic melanoma. N. Engl. J. Med. *364*, 2517–2526.
6. Hodi, F.S., O'Day, S.J., McDermott, D.F., Weber, R.W., Sosman, J.A., Haanen, J.B., Gonzalez, R., Robert, C., Schadendorf, D., Hassel, J.C., et al. (2010). Improved survival with ipilimumab in patients with metastatic melanoma. N. Engl. J. Med. *363*, 711–723.
7. Robert, C., Schachter, J., Long, G.V., Arance, A., Grob, J.J., Mortier, L., Daud, A., Carlino, M.S., McNeil, C., Lotem, M., et al. (2015). Pembrolizumab versus Ipilimumab in advanced melanoma. N. Engl. J. Med. *372*, 2521–2532.
8. Larkin, J., Lao, C.D., Urba, W.J., McDermott, D.F., Horak, C., Jiang, J., and Wolchok, J.D. (2015). Efficacy and safety of Nivolumab in patients with BRAF V600 mutant and BRAF wild-type advanced melanoma: a pooled analysis of 4 clinical trials. JAMA Oncol. *1*, 433–440.
9. Chandran, S.S., Somerville, R.P.T., Yang, J.C., Sherry, R.M., Klebanoff, C.A., Goff, S.L., Wunderlich, J.R., Danforth, D.N., Zlott, D., Paria, B.C., et al. (2017). Treatment of metastatic uveal melanoma with adoptive transfer of tumour-infiltrating lymphocytes: a single-centre, two-stage, single-arm, phase 2 study. Lancet Oncol. *18*, 792–802.
10. Betof Warner, A., Corrie, P.G., and Hamid, O. (2023). Tumor-infiltrating lymphocyte therapy in melanoma: facts to the future. Clin. Cancer Res. *29*, 1835–1854.
11. Soltantoyeh, T., Akbari, B., Karimi, A., Mahmoodi Chalbatani, G., Ghahri-Saremi, N., Hadjati, J., Hamblin, M.R., and Mirzaei, H.R. (2021). Chimeric antigen receptor (CAR) T cell therapy for metastatic melanoma: Challenges and road ahead. Cells *10*, 1450.
12. Seitter, S.J., Sherry, R.M., Yang, J.C., Robbins, P.F., Shindorf, M.L., Copeland, A.R., McGowan, C.T., Epstein, M., Shelton, T.E., Langhan, M.M., et al. (2021). Impact of prior treatment on the efficacy of adoptive transfer of tumor-infiltrating lymphocytes in patients with metastatic melanoma. Clin. Cancer Res. *27*, 5289–5298.
13. Yarza, R., Bover, M., Herrera-Juarez, M., Rey-Cardenas, M., Paz-Ares, L., Lopez-Martin, J.A., and Haanen, J. (2023). Efficacy of T-cell receptor-based adoptive cell therapy in cutaneous melanoma: A meta-analysis. Oncologist *28*, e406–e415.
14. Zaretsky, J.M., Garcia-Diaz, A., Shin, D.S., Escuin-Ordinas, H., Hugo, W., Hu-Lieskovan, S., Torrejon, D.Y., Abril-Rodriguez, G., Sandoval, S., Barthly, L., et al. (2016). Mutations associated with acquired resistance to PD-1 blockade in melanoma. N. Engl. J. Med. *375*, 819–829.
15. Jerby-Arnon, L., Shah, P., Cuoco, M.S., Rodman, C., Su, M.-J., Melms, J.C., Leeson, R., Kanodia, A., Mei, S., Lin, J.-R., et al. (2018). A cancer cell program promotes T cell exclusion and resistance to checkpoint blockade. Cell *175*, 984–997.e24.
16. Saleh, R., and Elkord, E. (2020). Acquired resistance to cancer immunotherapy: Role of tumor-mediated immunosuppression. Semin. Cancer Biol. *65*, 13–27.
17. Zhang, Y., Kurupati, R., Liu, L., Zhou, X.Y., Zhang, G., Hudaihed, A., Filisio, F., Giles-Davis, W., Xu, X., Karakousis, G.C., et al. (2017). Enhancing CD8+ T cell fatty acid catabolism within a metabolically challenging tumor microenvironment increases the efficacy of melanoma immunotherapy. Cancer Cell *32*, 377–391.e9.
18. Bedogni, B., and Powell, M.B. (2009). Hypoxia, melanocytes and melanoma - survival and tumor development in the permissive microenvironment of the skin. Pigment Cell Melanoma Res. *22*, 166–174.
19. Einarsdottir, B.O., Bagge, R.O., Bhadury, J., Jespersen, H., Mattsson, J., Nilsson, L.M., Truvé, K., López, M.D., Naredi, P., Nilsson, O., et al. (2014). Melanoma patient-derived xenografts accurately model the disease and develop fast enough to guide treatment decisions. Oncotarget *5*, 9609–9618.
20. Garman, B., Anastopoulos, I.N., Krepler, C., Brafford, P., Sproesser, K., Jiang, Y., Wubbenhorst, B., Amaravadi, R., Bennett, J., Beqiri, M., et al. (2017). Genetic and genomic characterization of 462 melanoma patient-derived xenografts, tumor biopsies, and cell lines. Cell Rep. *21*, 1936–1952.
21. Pearce, E.L. (2010). Metabolism in T cell activation and differentiation. Curr. Opin. Immunol. *22*, 314–320.
22. Vander Heiden, M.G., Cantley, L.C., and Thompson, C.B. (2009). Understanding the Warburg Effect: The metabolic requirements of cell proliferation. Science *324*, 1029–1033.
23. Kouidhi, S., Elgaaied, A.B., and Chouaib, S. (2017). Impact of metabolism in on T-cell differentiation and function and cross talk with tumor microenvironment. Front. Immunol. *8*, 270.
24. Ho, P.-C., Bihuniak, J.D., Macintyre, A.N., Staron, M., Liu, X., Amezquita, R., Tsui, Y.-C., Cui, G., Micevic, G., Perales, J.C., et al. (2015). Phosphoenolpyruvate is a metabolic checkpoint of anti-tumor T cell responses. Cell *162*, 1217–1228.
25. Kempkes, R.W.M., Joosten, I., Koenen, H.J.P.M., and He, X. (2019). Metabolic pathways involved in regulatory T cell functionality. Front. Immunol. *10*, 2839.
26. Fischer, K., Hoffmann, P., Voelkl, S., Meidenbauer, N., Ammer, J., Edinger, M., Gottfried, E., Schwarz, S., Rothe, G., Hoves, S., et al. (2007). Inhibitory effect of tumor cell-derived lactic acid on human T cells. Blood *109*, 3812–3819.
27. Pilon-Thomas, S., Kodumudi, K.N., El-Kenawi, A.E., Russell, S., Weber, A.M., Luddy, K., Damaghi, M., Wojtkowiak, J.W., Mulé, J.J., Ibrahim-Hashim, A., and Gillies, R.J. (2016). Neutralization of tumor acidity improves antitumor responses to immunotherapy. Cancer Res. *76*, 1381–1390.
28. Parry, R.V., Chemnitz, J.M., Frauwirth, K.A., Lanfranco, A.R., Braunstein, I., Kobayashi, S.V., Linsley, P.S., Thompson, C.B., and Riley, J.L. (2005). CTLA-4 and PD-1 receptors inhibit T-cell activation by distinct mechanisms. Mol. Cell. Biol. *25*, 9543–9553.
29. Patsoukis, N., Bardhan, K., Chatterjee, P., Sari, D., Liu, B., Bell, L.N., Karoly, E.D., Freeman, G.J., Petkova, V., Seth, P., et al. (2015). PD-1 alters T-cell metabolic reprogramming by inhibiting glycolysis and promoting lipolysis and fatty acid oxidation. Nat. Commun. *6*, 6692.
30. Cao, Y., Rathmell, J.C., and Macintyre, A.N. (2014). Metabolic reprogramming towards aerobic glycolysis correlates with greater proliferative ability and resistance to metabolic inhibition in CD8 versus CD4 T cells. PLoS One *9*, e104104.
31. Bwayi, M.N., Garcia-Maldonado, E., Chai, S.C., Xie, B., Chodankar, S., Huber, A.D., Wu, J., Annu, K., Wright, W.C., Lee, H.M., et al. (2022). Molecular basis of crosstalk in nuclear receptors: heterodimerization between PXR and CAR and the implication in gene regulation. Nucleic Acids Res. *50*, 3254–3275.
32. Doedens, A.L., Phan, A.T., Stradner, M.H., Fujimoto, J.K., Nguyen, J.V., Yang, E., Johnson, R.S., and Goldrath, A.W. (2013). Hypoxia-inducible factors enhance the effector responses of CD8(+) T cells to persistent antigen. Nat. Immunol. *14*, 1173–1182.
33. Grabacka, M.M., Wilk, A., Antonczyk, A., Banks, P., Walczyk-Tytko, E., Dean, M., Pierzchalska, M., and Reiss, K. (2016). Fenofibrate induces ketone body production in melanoma and glioblastoma cells. Front. Endocrinol. *7*, 5.
34. Panigrahy, D., Kaipainen, A., Huang, S., Butterfield, C.E., Barnés, C.M., Fannon, M., Laforme, A.M., Chaponis, D.M., Folkman, J., and Kieran, M.W. (2008). PPARα agonist fenofibrate suppresses tumor growth through direct and indirect angiogenesis inhibition. Proc. Natl. Acad. Sci. USA *105*, 985–990.
35. Gemta, L.F., Siska, P.J., Nelson, M.E., Gao, X., Liu, X., Locasale, J.W., Yagita, H., Slingluff, C.L., Hoehn, K.L., Rathmell, J.C., and Bullock, T.N.J. (2019). Impaired enolase 1 glycolytic activity restrains effector functions of tumor-infiltrating CD8 $^{+}$ T cells. Sci. Immunol. *4*, eaap9520.

36. Hersey, P., Watts, R.N., Zhang, X.D., and Hackett, J. (2009). Metabolic approaches to treatment of melanoma. Clin. Cancer Res. *15*, 6490–6494.

37. Jaune, E., and Rocchi, S. (2018). Metformin: Focus on melanoma. Front. Endocrinol. *9*, 472.

38. Finisguerra, V., Dvorakova, T., Formenti, M., Van Meerbeeck, P., Mignion, L., Gallez, B., and Van Den Eynde, B.J. (2023). Metformin improves cancer immunotherapy by directly rescuing tumor-infiltrating CD8 T lymphocytes from hypoxia-induced immunosuppression. J. Immunother. Cancer *11*, e005719.

39. Wang, R., Li, Y., Zhao, Y., Shi, F., Zhou, Q., Wu, J., Lyu, S., and Song, Q. (2022). Metformin inducing the change of functional and exhausted phenotypic tumor-infiltrated lymphocytes and the correlation with JNK signal pathway in triple-negative breast cancer. Breast Cancer *14*, 391–403.

40. Zhang, Y., and Ertl, H.C. (2014). The effect of adjuvanting cancer vaccines with herpes simplex virus glycoprotein D on melanoma-driven $CD8^+$ T cell exhaustion. J. Immunol. *193*, 1836–1846.